International Conference on Electrical, Computer, Communications and Mechatronics Engineering (ICECCME 2022)

CONFERENCE PROCEEDINGS

16-18 November 2022

Male, Maldives

Proc. of the International Conference on Electrical, Computer, Communications and Mechatronics Engineering (ICECCME)
16-18 November 2022, Maldives

Active sensors for UAV autonomous navigation on Amazon region

Roberto N. Salles
dept. of C4ISR
Institute for Advanced Studies
São José dos Campos, Brazil
salles@ieav.cta.br

Haroldo F. de Campos Velho
lab. of applied computing and mathematics
Institute for Space Research
São José dos Campos, Brazil
haroldo.camposvelho@inpe.br

Elcio H. Shiguemori
dept. of C4ISR
Institute for Advanced Studies
São José dos Campos, Brazil
elcio@ieav.cta.br

***Abstract*—This work is an additional exploration inspired by the results of an earlier study of the geo-localization problem over a densely forested region of the Brazilian Amazon forest. Light Detection and Ranging (LiDAR) data was post-processed from 3D cloud point format to 2D elevation images and template matching was used with normalized cross-correlation. Within a constrained search area it was possible to geo-localize the 2D patches of surface images on Interferometric Synthetic Aperture Radar (InSAR) elevation data. The transect 3D cloud point was transformed into a 12.5m resolution 2D surface image with the circular binning procedure, a resolution compatible with the Advanced Land Observation Satellite (ALOS) elevation maps used as reference. This application of template matching achieved 36m root mean square error, or about 4 pixels of error, over the LiDAR transect route. Position estimation is essential for autonomous navigation of aerial vehicles, and experiments with LiDAR data show potential for localization over densely forested regions, where Computer Vision methods using optical camera data may fail to acquire distinguishable features.**

***Index Terms*—aerial drone, autonomous navigation, template matching, LiDAR data, InSAR images**

I. Introduction

Autonomous navigation of Unmanned Aerial Vehicles (UAV) is a desirable capability in science, engineering, and many other applications. It is commonly achieved by combining readings from an Inertial Motion Unit (IMU) and a Global Navigation Satellite System (GNSS), such as the Global Positioning System (GPS) [1]. The combination is desirable because position estimations using only an IMU will deviate from the real position of a moving vehicle. This happens because an IMU doesn't measure positions directly but accelerations and angular velocities, that must first be integrated along with the small measurement errors to generate a path. An UAV may also drift due to a constant wind, a difficult deviation to detect and compensate without additional inputs [2]. A positioning system such as GPS provides positions without the drawback of the ever increasing deviation of an IMU but the GNSS-derived measurements tend to be sparser. The combination of an IMU and a GNSS on a UAV provides good position estimations with fine sensibility, derived from the IMU, and with bounded uncertainty, derived from the GNSS. A drone designed in such a way can, therefore, go to geographical locations by applying appropriate corrections to its control system to keep itself on its desired route.

The usefulness of this established solution is dependant on the reliability of each positioning system used. GNSS signals are of particular importance – without them the uncertainty of the system becomes the uncertainty of the IMU, i.e. unbounded in time. There are multiple reasons why the GNSS signals may become unavailable or unreliable, for instance, through interference. Malicious interference of the GNSS signals, such as jamming and spoofing [3], can be mitigated by the use of better antennas, spacial and frequency filtering, and vector tracking [4]. Outages and denial of service can be mitigated by the use of more than one GNSS. An UAV is also subject to natural phenomena interference [5]–[7]. One natural phenomenon directly associated with the signal interference of a GNSS is the ionospheric scintillation [8]–[11]. It is characterized by irregularities in the atmospheric electronic density. The ionospheric scintillation may cause the complete disruption of GNSS signals [12]–[14]. Ionospheric bubbles [15]–[17] are events linked to the scintillation phenomenon. They mostly occur on the equatorial magnetic zone on the Earth, including the northern region of Brazil [18].

Alternatively to a GNSS, Computer Vision (CV) techniques have been applied to provide position estimations. Multiple approaches exist depending on the imaged scene and on the utilized sensor. Recent approaches may use Convolutional Neural Networks [19] and can estimate positions using the simple down-facing RGB cameras present in many UAV, or specific sensors may be needed depending on the circumstances or scene, for example a thermal imaging sensor for night position estimation [20], or a Light Detection and Ranging (LiDAR) sensor for position estimation over coastal regions [21].

The Amazon forest region is a challenging area of study for autonomous navigation. It presents a scenario of multiple difficulties at once. First, it is near the magnetic equator (Fig. 1, top), where the influence of ionospheric effects (e.g. ionospheric bubbles) is most accentuated. The GNSS signals

978-1-6654-7095-7/22/$31.00 ©

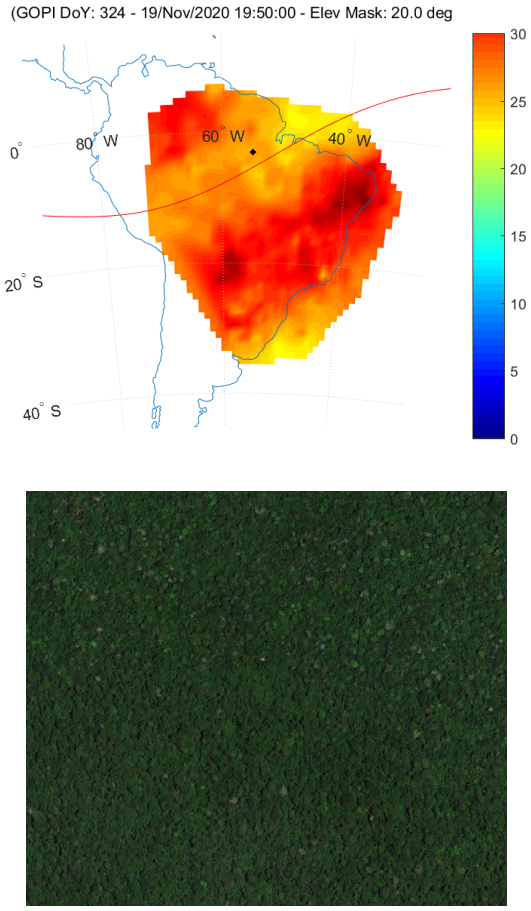

Fig. 1. An example of the Total Electron Content (TEC) map over South America is shown on the top, displaying the magnetic equator (red line) and the location of the study (black dot). Strong variation on TEC values can affect the radio wave transmissions, including GNSS. On the bottom, an image for the visible band over the location of the study on the Amazon forest, showing no distinguishable features. TEC is a good parameter to monitor for possible space weather impacts. TEC is measured in electrons per square meter. By convention, 1 TEC Unit $TECU = 10^{16}$ electrons/m^2. Vertical TEC values in Earth's ionosphere can range from a few to several hundred TECU.

might be completely disrupted and unavailable for use due to the phenomena, making the CV an attractive alternative or redundancy. Second, the forest presents an uniformity of visual features (Fig. 1, bottom), i.e. distinguishing features are scarce and, consequently, problematic for multiple CV techniques that work really well on urban or mixed scenarios.

The LiDAR sensor can be used for navigation aid when LiDAR mappings are available [22], but LiDAR mappings of the Amazon region are almost nonexistent. Most of the existing elevation maps were derived from Interferometric Synthetic Aperture Radar (InSAR) data due to the large extent of the forest and the usual presence of clouds. This work explores how height data from the active sensor LiDAR can be related and used against elevation maps generated from an InSAR to estimate positions. A small flight trajectory error is obtained on a LiDAR transect used for testing the proposed methodology, presenting a 36 m root mean square error (RMSE), an acceptable deviation for many critical missions over the region.

The next section, Theory and Methods, explore basic concepts of LiDAR, InSAR, template matching, and how to make both data compatible for position estimation. The Experiment and Results section describes the experiment made by post-processing LiDAR data from the Amazon region, and it is followed by Discussion and Conclusion section, where differences from the original experiment are considered.

II. Theory and Methods

A. The LiDAR sensor

An airborne LiDAR sensor is an optical and active sensor built with a laser unit that emits laser pulses and is able to record its reflections, translating those to distances, and an oscillating mirror that regularly changes the laser pointing direction. Current LiDAR sensors are able to record the whole reflection history and are called full waveform LiDAR. More commonly, LiDAR sensors process and record the reflections over an intensity threshold and are called discrete-return LiDAR. The combined information of vehicle attitude, laser pointing direction and range measured produces a gridless 3D point set called cloud point data. Although of optical origin, the 3D cloud point data is not readily usable with standard CV techniques dealing with 2D images. The data must first be transformed from a 3D point list to a fixed grid 2D image.

B. The SAR sensor and the InSAR

The Synthetic Aperture Radar (SAR) is an active sensor that uses side-looking antennas to emit microwave pulses and to read the backscatter while the platform moves, combining the multiple readings into a synthetic aperture (i.e. a larger antenna) for better resolution. The Interferometric SAR (InSAR) combines two single-look complex images generated from SAR with a predefined separation (baseline), unwrapping the phase differences into an elevation model [23].

This simplified description serves two purposes here. The first is to illustrate how different from LiDAR the generated elevation maps of InSAR are at the origin of the process [24]. Secondly, it is considered that SAR sensors with longer wavelengths have better penetration on forested areas, corresponding well to the underlying terrain, but this has not been our experience when comparing it to LiDAR derived terrains on the Amazon region, at least regarding the shape of the measured elevations. In fact, this is the reason why the surface elevation model of LiDAR, related to the canopy of trees, is used instead of the terrain one in this work (see Section IV).

1) LiDAR and InSAR data: Fig. 2 illustrates a discrete-return airborne LiDAR laser pulse interacting with a tree. It records three reflections, the distances measured shown as dots. Surface maps, including the canopy, are created from the first reflections (gray dot) while terrain maps are created considering the last reflections (green dot). Intermediate reflections may occur (red dot) and may be recorded by discreet-return LiDAR sensors capable of registering more than two returns. At the same time, two distinct near orbit captures of an InSAR satellite system is shown. Two SAR backscatters are

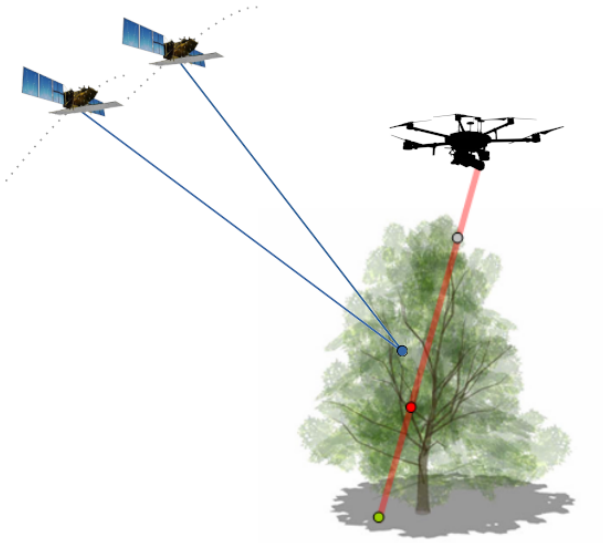

Fig. 2. Aerial vehicle equipped with a LiDAR sensor. The first reflection (gray dot) is used for surface mapping and the last reflection (green dot) is used for terrain mapping. Satellite InSAR data is also captured (blue dot).

combined and processed to estimate a height position from a ground plane or rougher terrain model, and is shown as the blue dot in the illustration.

C. Position estimation by template matching

In general, the template matching algorithm takes a smaller image, called the template, against a larger image, called the reference, usually through cross-correlation or a resembling method, producing a map of similarities, where the position of the greatest correlation (i.e. similarity) is assumed as the position estimation. The search is exhaustive on the reference image and the speed and memory costs increase if the size of the template or the size of the reference image are increased. When the reference image is geo-referenced, the estimated pixel position can be translated to a geographic location.

Figure 3 illustrates the template matching algorithm. The measurement of similarity used was the normalized cross-correlation. Although cross-correlation can be used, it is not well suited for the template matching of elevation estimations, as explained later. Equations 1 and 2 use the same notation displayed on Fig 3.

1) Cross-Correlation limitations on elevation data: The Cross-Correlation (CC) is a well known similarity measurement for image matching between a template and a reference. It is defined as

$$c(s,t) = \sum_{x,y} f(x,y)\, w(x-s, y-t) \tag{1}$$

where f is a reference 2D image of dimensions $M \times N$, w is the template (or window) of dimensions $J \times K$, smaller than $M \times N$, that is being cross-referenced and c is the cross-correlation result. The translation from origin is estimated from the corresponding pair (s,t) where the value of c is

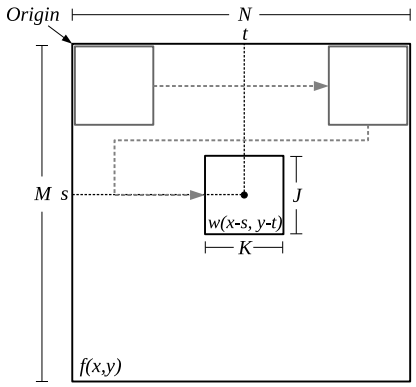

Fig. 3. Reference f (InSAR) and template window w (LiDAR).

greatest. This approach is only valid when the different regions of the reference image have similar average values [25]. Elevation images have naturally occurring regions of lower and higher average values corresponding to valleys and mountains, invalidating the assumption and skewing the results towards higher average regions.

2) Normalized Cross-Correlation alternative: The Normalized Cross-Correlation (NCC) adjusts cross-correlation for regions of different average values, and the result is better estimations in terms of correlating the shape of terrain or surface maps, the essential information for geo-localization. It is defined as

$$ncc(s,t) = \frac{\sum_{x,y}[f(x,y) - \bar{f}_{s,t}][w(x-s,y-t) - \bar{w}]}{\sqrt{\sum_{x,y}[f(x,y) - \bar{f}_{s,t}]^2 \sum_{x,y}[w(x-s,y-t) - \bar{w}]^2}} \tag{2}$$

where the numerator is the same as the cross-correlation presented earlier minus the average of the region under the template $\bar{f}_{s,t}$ and minus the constant average of the template or window $\bar{w}$. The denominator normalizes the adjusted values producing results $ncc(s,t)$ on the range [-1,1], where 1 means the same feature was found, 0 means completely unrelated features, and -1 means an inverted feature was found. The latter only occurs when negative values exist therefore, for most of elevation reference maps and templates, the expected range is actually [0,1]. Note that the NCC is not computable flat surfaces.

D. Compatibilization of LiDAR and InSAR data

InSAR geo-referenced elevation maps are 2D images where geographical coordinates can be obtained for each pixel position. Pixels have a spacial resolution, called pixel spacing, and an associated value, in this case the elevation itself. Differently, LiDAR 3D cloud point data must first be transformed into a 2D image of compatible characteristics, i.e. a regular grid of same orientation and pixel spacing. This process is called binning [26], and it is employed for the application of the template matching algorithm.

For each LiDAR point coordinate, a corresponding bin is located, and the elevation value of the point is attributed as

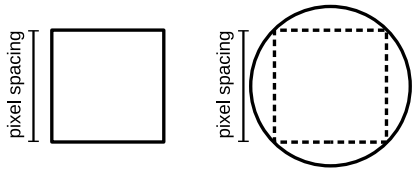

Fig. 4. The pixel spacing defines an exact square bin. Conversely, by defining a bin size, a 2D matrix can be generated to accommodate LiDAR point values. A circular bin (right) allow points that would be outside the pixel spacing defined area to influence the matrix generation.

the value of the bin if null, or if greater or less than the previous value. Keeping the greatest values result in a surface 2D elevation map and keeping the lowest values result in a 2D terrain elevation map. As Fig. 4 shows, the bin is not necessarily limited to a square bin exactly representing the pixel limits and in this work a circular bin was used.

E. Flowchart of the geo-localization procedure

Figure 5 illustrates the whole procedure of position estimation applied using 3D LiDAR cloud point data over an InSAR reference image.

1. The LiDAR transect to be post-processed is selected and the largest template that fits on its width is established based on the reference image resolution. In this work the reference image resolution was 12.5m so a safe size for the template of 30×30 pixels.
2. The cloud point data is processed through binning with the intention of generating a surface elevation map, i.e. a 2D representation of the canopy is generated.
3. The generated data is sampled according to the trajectory into templates for matching.
4. Each template is searched using the template matching algorithm with NCC against the InSAR reference image and the highest peak of correlation is assumed as the position estimation.
5. The center pixel position can be translated to a geographic coordinate.

The template matching search can be limited to an area where the UAV is expected to be, such as an area around the IMU estimated position. The most immediate benefit is to hasten and save computing resources, but limiting the search area also improve the rate of correct matches. Considering the assumed position of the UAV, a limited search around it can be established.

In this work, an area half the size of the template was searched (around 180m).

III. Location and Data

The area of this study is approximately 4×4 km and located on the Tapajós National Reserve (Fig 6). Of the nine LiDAR transects originally acquired on that region by the EBA project[1] the transect NP_T-1016-001 was selected to reproduce an earlier experiment [22], but this time over an InSAR elevation reference map of low resolution, instead of the LiDAR derived map. The LiDAR sensor specifications and setup for the EBA dataset acquisition are listed on Table I.

The InSAR elevation map used as the reference image for the experiment has been acquired as part of the Advanced Land Observation Satellite (ALOS) mission, by using the

[1]The LiDAR transects are part of Estimating the Biomass of Amazon (EBA) project from CCST/INPE. They are named NP_T-1016-001 to NP_T-1016-009. The authors would like to thank the project coordinator Dr. Jean Ometto for the access to this data.

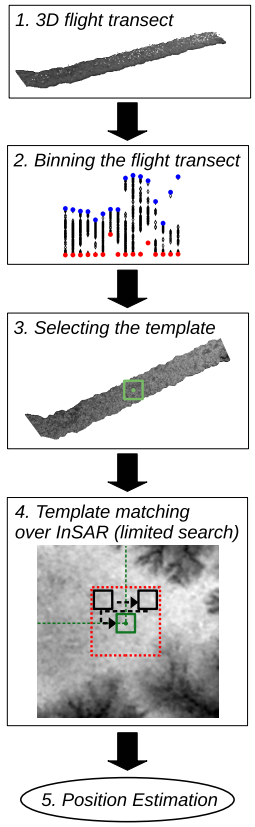

Fig. 5. The flowchart of the experiment. Source data is transformed from 3D to 2D through binning and templates (green) are used against the InSAR reference, through template matching, producing an estimated translation on x/y axis, that can be converted to a position or geographic coordinate. The search can be in the full reference image or limited to an assumed sufficient area of search (the encompassing dotted red area).

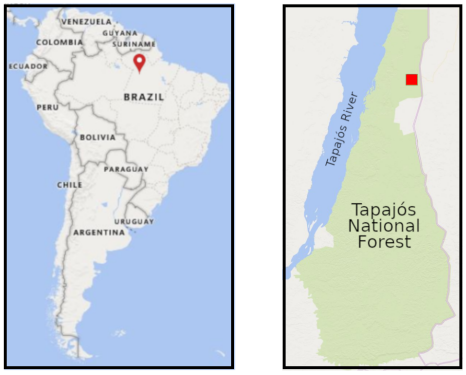

Fig. 6. Location of the experiment with ever increasing detail. Last image shows the combined LiDAR cloud point intensity rendered over a satellite image.

TABLE I.
TRIMBLE HARRIER 68i LiDAR SYSTEM SPECIFICATIONS.

Specification	Value
LiDAR sensor	HARRIER 68i
Wavelength	1550nm
Scan frequency	5 Hz to 200 Hz
Field of view	Up to 30^o
Pulse density requested	4 pulses / m^2
Footprint	30 cm
Flying height	600 m
Track width on the ground	494 m (avg)

data from the Phased Array type L-band Synthetic Aperture Radar (PALSAR) sensor, which enables day-and-night and all-weather land observation. The ALOS satellite was launched on January 24, 2006. The terrain corrected product is derived from a single look complex SAR image pair. It is provided in UTM coordinates and is corrected for terrain by using SRTMGL1 - Shuttle Radar Topography mission at 30m resolution. Additional corrections by the Alaska Satellite Facility (June 2015, version 1.1), responsible for the distribution.

All computations involving geographical coordinates were done using the Universal Transverse Mercator (UTM) coordinate system. The LiDAR and InSAR data were considered to be correctly corregistered as provided, after careful inspection.

IV. Experiment Description and Results

The experiment is an alternative exploration of the flight transect used in [22] where the following differences must be noted. i) An ALOS InSAR elevation map was used as the reference image, instead of a combination of LiDAR transects; ii) The ALOS InSAR elevation reference covers the flight transect completely, including where previously there was no LiDAR reference data on the beginning and end of the flight transect; iii) The pixel spacing resolution of the 2D images is 12.5m instead of 5m; and iv) Due to the lower resolution, the template windows used were adapted to 30×30, instead of 70×60. Other aspects remain the same, with the exception of the lower total number of systematic templates generated throughout the route, an inevitability of the lower 12.5 m resolution. In particular, it must be noted that the x-axis of Fig. 8, if compared to similar graphs on the earlier work, represent the same total distance.

The trajectory is a straight line with no deviation, using only the transect NP_T-1016-001 as a source of LiDAR data. Figure 7 illustrates the straight line route (red), along with the estimated positions by template matching (blue). A limited search was used with a search area of 187 m, or half the size of the template window, around the template.

A graph similar to the ones of the earlier study is shown on Fig. 8. The normalized cross-correlation value of the matches is very high (NCC(max), orange) but, in this LiDAR×InSAR study, doesn't ensure a good matching. The worse correlation values for each application of the algorithm is also displayed (NCC(min), yellow), for comparison. The estimated errors are shown in blue, in the form of the Euclidian distance (pixels).

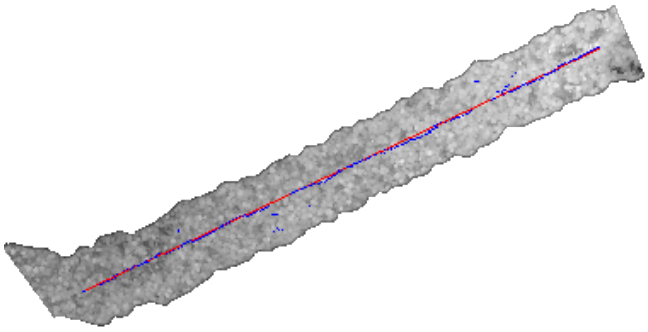

Fig. 7. Flight transect with route in red and estimated positions using template matching in blue. The estimations were plotted as dots and are not connected.

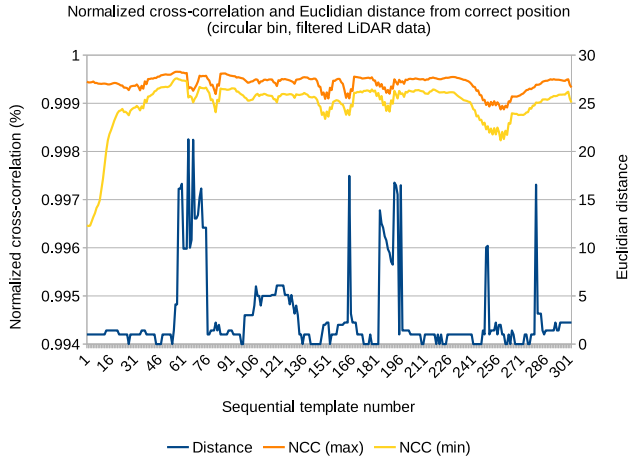

Fig. 8. Position estimation errors of the template matching algorithm (blue) and respective NCC values, highest (orange) and lowest (yellow).

Table II summarizes and displays the root mean square error and the standard deviation for the whole flight route in pixel values and in meters. Although the achieved error of 36 m is rather large and around five times the error of the earlier study (7 m of error), it is only around three pixels of lower resolution. In one hand, one important difference is that the earlier LiDAR×LiDAR study used the whole reference image with very good results. On the other hand, the lack of LiDAR coverage on the Amazon region makes the template matching with InSAR data an interesting alternative, as free low resolution InSAR data exists covering all the Amazon. InSAR elevation maps of better resolution could be used, if available, with the expectation of reduced matching errors.

TABLE II.
ESTIMATION ERRORS FOR THE EXPERIMENT.

Search Range	RMSE	STDDEV
Limited (pixels)	2.87	4.17
Limited (meters)	35.92m	52.12m

V. Discussion and Conclusion

The results using data from the experiment indicate that it is possible to correlate LiDAR surface data with InSAR elevation maps for aid in navigation over a densely forested region of the Brazilian Amazon forest. In that region, visual aid techniques using RGB cameras may fail to acquire distinguishing features. The occurrence of ionospheric scintillation events can generate interference or even inhibit the use of GNSS signals for positioning. The main contribution of this work is to approach the difficult problem of geo-localization over a densely forested region of the Brazilian Amazon while adapting the earlier experiment to use an InSAR reference image.

The results of this experiment were limited by the low resolution of the InSAR elevation maps, as the LiDAR data could easily be scaled for use with better resolution InSAR elevation maps. Conversely, InSAR elevation maps of lower resolution are plentiful and were proved sufficient for basic guidance on that difficult region. Imposing a restriction of the search area of template matching algorithm was essential to eliminate bad matches and to better estimate positions. It is possible to notice that, while the proposed solution works most of the time, there are still areas where geo-localization is not achieved, even with the constraint of the search area. It must be noted, however, that the flight transect is over a very plain region of the forest.

References

[1] G. Balamurugan, J. Valarmathi, and V. P. S. Naidu, "Survey on uav navigation in gps denied environments," in *2016 International Conference on Signal Processing, Communication, Power and Embedded System (SCOPES)*, 2016, pp. 198–204.

[2] M. Koifman and I. Y. Bar-Itzhack, "Inertial navigation system aided by aircraft dynamics," *IEEE transactions on control systems technology*, vol. 7, no. 4, pp. 487–493, 1999.

[3] A. Hamza, U. Akram, A. Samad, S. N. Khosa, R. Fatima, and M. F. Mushtaq, "Unmaned aerial vehicles threats and defence solutions," in *2020 IEEE 23rd International Multitopic Conference (INMIC)*, 2020, pp. 1–6.

[4] G. X. Gao, M. Sgammini, M. Lu, and N. Kubo, "Protecting gnss receivers from jamming and interference," *Proceedings of the IEEE*, vol. 104, no. 6, pp. 1327–1338, 2016.

[5] P. Cilliers, B. Opperman, and R. Meyer, "Investigation of ionospheric scintillation over south africa and the south atlantic anomaly using gps signals: First results," in *2009 IEEE International Geoscience and Remote Sensing Symposium*, vol. 2. IEEE, 2009, pp. II–879.

[6] T.-H. Kim, C. S. Sin, and S. Lee, "Analysis of effect of spoofing signal in gps receiver," in *2012 12th International Conference on Control, Automation and Systems*. IEEE, 2012, pp. 2083–2087.

[7] T.-H. Kim, C. S. Sin, S. Lee, and J. H. Kim, "Analysis of effect of anti-spoofing signal for mitigating to spoofing in gps l1 signal," in *2013 13th International Conference on Control, Automation and Systems (ICCAS 2013)*. IEEE, 2013, pp. 523–526.

[8] E. F. Aon, A. R. Othman, Y. H. Ho, and R. Shaddad, "Analysis of gps link ionospheric scintillation during solar maximum at utem, malaysia," in *2014 IEEE 2nd International Symposium on Telecommunication Technologies (ISTT)*. IEEE, 2014, pp. 84–87.

[9] W. A. Ahmed, F. Wu, and G. I. Agbaje, "Analysis of gps ionospheric scintillation during solar maximum at mid-latitude," in *2016 IEEE International Geoscience and Remote Sensing Symposium (IGARSS)*. IEEE, 2016, pp. 4151–4154.

[10] X. Sun, Z. Zhang, Y. Ji, S. Yan, W. Fu, and Q. Chen, "Algorithm of ionospheric scintillation monitoring," in *2018 7th International Conference on Digital Home (ICDH)*. IEEE, 2018, pp. 264–268.

[11] I. Gulati, H. Li, S. Stainton, M. Johnston, and S. Dlay, "Investigation of ionospheric phase scintillation at middle-latitude receiver station," in *2019 International Symposium ELMAR*. IEEE, 2019, pp. 191–194.

[12] S. Datta-Barua, P. Doherty, S. Delay, T. Dehel, and J. A. Klobuchar, "Ionospheric scintillation effects on single and dual frequency gps positioning," in *Proceedings of the 16th International Technical Meeting of the Satellite Division of The Institute of Navigation (ION GPS/GNSS 2003)*, 2003, pp. 336–346.

[13] R. Steenburgh, C. Smithtro, and K. Groves, "Ionospheric scintillation effects on single frequency gps," *Space Weather*, vol. 6, no. 4, 2008.

[14] K. Guo, M. Aquino, and S. V. Veettil, "Ionospheric scintillation intensity fading characteristics and gps receiver tracking performance at low latitudes," *GPS Solutions*, vol. 23, no. 2, pp. 1–12, 2019.

[15] B. Carter, J. Retterer, E. Yizengaw, K. Wiens, S. Wing, K. Groves, R. Caton, C. Bridgwood, M. Francis, M. Terkildsen *et al.*, "Using solar wind data to predict daily gps scintillation occurrence in the african and asian low-latitude regions," *Geophysical Research Letters*, vol. 41, no. 23, pp. 8176–8184, 2014.

[16] M. Mokhtar, N. Rahim, M. Ismail, and S. Buhari, "Ionospheric perturbation: A review of equatorial plasma bubble in the ionosphere," in *2019 6th International Conference on Space Science and Communication (IconSpace)*. IEEE, 2019, pp. 23–28.

[17] H. Takahashi, M. J. Taylor, J. Sobral, A. Medeiros, D. Gobbi, and D. Santana, "Fine structure of the ionospheric plasma bubbles observed by the oi 6300 and 5577 airglow images," *Advances in Space Research*, vol. 27, no. 6-7, pp. 1189–1194, 2001.

[18] D. Silva, H. Takahashi, C. Wrasse, and C. Figueireido, "Characteristics of ionospheric bubbles observed by tec maps in brazilian sector," in *15th International Congress of the Brazilian Geophysical Society*. IEEE, 2017.

[19] H. Goforth and S. Lucey, "Gps-denied uav localization using pre-existing satellite imagery," in *2019 International Conference on Robotics and Automation (ICRA)*, 2019, pp. 2974–2980.

[20] W. Silva, E. H. Shiguemori, N. L. Vijaykumar, and H. F. Campos Velho, "Estimation of uav position with use of thermal infrared images," in *International Conference on Sensing Technology (ICST-2015)*, Auckland, New Zealand: School of Engineering and Advanced Technology – Massey University, 2015, pp. 211–217.

[21] J. R. G. Braga, H. F. Campos Velho, G. Conte, P. Doherty, and E. H. Shiguemori, "An image matching system for autonomous uav navigation based on neural network," in *2016 14th International Conference on Control, Automation, Robotics and Vision (ICARCV)*. IEEE, 2016, pp. 1–6.

[22] R. N. Salles, H. F. Campos Velho, and E. H. Shiguemori, "Automatic position estimation based on lidar $\times$ lidar data for autonomous aerial navigation in the amazon forest region," *Remote Sensing*, vol. 14, no. 2, 2022. [Online]. Available: https://www.mdpi.com/2072-4292/14/2/361

[23] R. GENS and J. L. V. GENDEREN, "Review article sar interferometry—issues, techniques, applications," *International Journal of Remote Sensing*, vol. 17, no. 10, pp. 1803–1835, 1996.

[24] H. Wang, H. Fu, J. Zhu, Z. Liu, B. Zhang, C. Wang, Z. Li, J. Hu, and Y. Yu, "Estimation of subcanopy topography based on single-baseline tandem-x insar data," *Journal of Geodesy*, vol. 95, no. 7, pp. 1–19, 2021.

[25] J. Lewis, "Fast template matching," *Vision Interface*, pp. 120–123, 1995.

[26] G. Hemann, S. Singh, and M. Kaess, "Long-range gps-denied aerial inertial navigation with lidar localization," in *2016 IEEE/RSJ International Conference on Intelligent Robots and Systems (IROS)*. IEEE, 2016, pp. 1659–1666.